Inorg. Chem. **2002**, *41*, 538–545

$Zr_{11}Sb_{18}$: A New Binary Antimonide Exhibiting an Unusual Sb Atom Network with Nonclassical Sb–Sb Bonding

Ingrid Elder, Chi-Shen Lee, and Holger Kleinke*

Department of Chemistry, University of Waterloo, Waterloo, Ontario, Canada N2L 3G1

Received August 1, 2001

The herewith-introduced antimonides $Zr_{11}Sb_{18}$ and $Zr_{10.4}V_{0.6}Sb_{18}$ were prepared by high-temperature techniques; both arc-melting and solid-state reactions at 1200 °C starting from α-$ZrSb_2$ and the metals Zr and V in powder form are possible methods. These isostructural compounds represent an unprecedented metal:antimony ratio of 11:18 and form a new structure type. $Zr_{11}Sb_{18}$ crystallizes in the tetragonal space group $I\bar{4}2d$, with the lattice dimensions $a = 676.94(4)$ pm and $c = 6007.3(5)$ pm, while the V-containing phase forms a slightly smaller unit cell with $a = 676.48(8)$ pm and $c = 6005.6(9)$ pm ($Z = 4$). Their structures are comprised of an Sb atom substructure with several intermediate Sb–Sb bonds starting at 311 pm, which is reminiscent of that found in the series $(Ti,M)_5Sb_8$ (M = Zr, Hf, Nb, Mo) published last year. Interwoven with this network is the Zr atom network, which forms a diamond-like metal atom substructure with long Zr–Zr contacts of ca. 360 pm. Band structure calculations based on the linear muffin tin orbital approach reveal these antimonides to be mainly stabilized by strong M–Sb and intermediate Sb–Sb bonds, and additionally—to the smallest extent—by M–M bonds (M = Zr, V). In agreement with the electronic structure calculations, $Zr_{11}Sb_{18}$ is metallic with a small positive Seebeck coefficient.

Introduction

Probably the best known antimonides are the filled skutterudites LnM_4Sb_{12} (Ln = lanthanoid, M = Fe, Co, Ni, ...),[1] for some representatives have outstanding thermoelectric properties as published five years ago in *Science*.[2] This discovery has caused many subsequent investigations into the skutterudite family.[3−5] The extraordinary thermoelectric properties of $LaFe_3CoSb_{12}$, a small-gap semiconductor,[2] result from a moderate Seebeck coefficient, a relatively good electrical conductivity, and a very low thermal conductivity. The latter is a consequence of the *rattling* of the Ln atom situated in a large icosahedral void of the three-dimensional Sb atom network.

We are currently exploring early-transition-metal antimonides with the long-term goal of discovering comparable Sb atom substructures in semiconducting antimonides. So far, the formation of semiconductors in this class appears to be the more difficult task, for we already uncovered two such structures in new *metallic* antimonides, namely, $Zr_2V_6Sb_9$[6] and $Ti_{5-\delta}M_\delta Sb_8$ (M = Zr, Hf, Nb, Mo).[7] Metallic properties usually prohibit use in the thermoelectric energy conversion due to too low Seebeck coefficients. However, the band structure of Ti_5Sb_8 revealed that a band gap may be achievable by heavy doping, e.g., replacing Sb atoms by Te and/or Ti by Mo atoms in the right concentration.

Subsequently, we investigated these and other systems with a metal:metalloid ratio of 5:8, with the metal atoms being early transition metals such as titanium, zirconium, vanadium, and molybdenum, and the metalloids (semimetals) being antimony, selenium, and tellurium. Thereby, we uncovered the new zirconium vanadium antimonide $Zr_{10.4}V_{0.6}Sb_{18}$, which crystallizes in a hitherto unreported structure type resembling the $(Zr,Ti)_5Sb_8$ structure published most recently. These two antimonide structures may be considered to form a new antimonide series, which is related to the Nowotny chimney ladder phases, but exhibits very different valence-electron concentrations.[8−10]

* To whom correspondence should be addressed. Fax:+1 (519) 746-0435. E-mail: kleinke@uwaterloo.ca.

(1) Jeitschko, W.; Braun, D. *Acta Crystallogr.* **1977**, *B33*, 7.
(2) Sales, B. C.; Mandrus, D.; Williams, R. K. *Science* **1996**, *272*, 1325.
(3) Nolas, G. S.; Morelli, D. T.; Tritt, T. M. *Annu. Rev. Mater. Sci.* **1999**, *29*, 89.
(4) Nolas, G. S.; Kaeser, M.; Littleton IV, R. T.; Tritt, T. M. *Appl. Phys. Lett.* **2000**, *77*, 1855.
(5) Dilley, N. R.; Bauer, E. D.; Maple, M. B.; Dordevic, S.; Basov, D. N.; Freibert, F.; Darling, T. W.; Migliori, A.; Chakoumakos, B. C.; Sales, B. C. *Phys. Rev.* **2000**, *B61*, 4608.
(6) Kleinke, H. *Eur. J. Inorg. Chem.* **1998**, 1369.
(7) Kleinke, H. *Inorg. Chem.* **2001**, *40*, 95.

10.1021/ic0108235 CCC: $22.00
Published on Web 01/11/2002

$(Zr,V)_{11}Sb_{18}$ is the fourth zirconium vanadium antimonide discovered in our group, after $(Zr,V)_{13}Sb_{10}$,[11] $(Zr,V)_{11}Sb_8$,[12] and $Zr_2V_6Sb_9$.[6] Our studies of its phase width revealed that (i) this is the most V-rich representative of this structure and (ii) this compound can actually be synthesized without vanadium! Thus, we herewith introduce also *a new binary zirconium antimonide*, namely, $Zr_{11}Sb_{18}$, with a Zr:Sb ratio between that of ZrSb and $ZrSb_{1.96}$ (β-$ZrSb_2$).[13] In this paper, we present the crystal and electronic structure of $Zr_{11-\delta}V_\delta Sb_{18}$ (with $0 \le \delta \le 0.6$) along with the thermopower of $Zr_{11}Sb_{18}$.

Experimental Section

Synthesis. The new compounds $Zr_{11}Sb_{18}$ and $Zr_{10.4}V_{0.6}Sb_{18}$ were prepared by high-temperature techniques, namely, arc-melting as well as annealing in tantalum crucibles at 1200 °C. Since antimony in its elemental form exhibits a high vapor pressure during arc-melting on one hand and a high reactivity in its molten state toward the reaction container material (tantalum) on the other hand, we initially synthesized α-$ZrSb_2$[14] in a fused silica tube starting from the elements at 650 °C, i.e., slightly above the melting point of antimony. Next, we added additional zirconium and vanadium powder in different ratios aiming at hypothetical "$Zr_{5-\delta}V_\delta Sb_8$" with $\delta = 1-4$, according to the following equation:

$$4ZrSb_2 + (1-\delta)Zr + \delta V \rightarrow Zr_{5-\delta}V_\delta Sb_8$$

These four mixtures were separately pressed into pellets, and then placed in tantalum tubes that were closed on one side. Under a flow of argon, the tubes were then sealed on the opposite side by melting the tantalum in an arc-welder. The filled Ta tubes were subsequently annealed at 1200 °C over a period of 72 h under a dynamic vacuum of 10^{-6} mbar.

Except for the reaction with $\delta = 1$, all mixtures were completely identified to contain the known binary antimonides and $Zr_2V_6Sb_9$ only. Conversely, most of the powder diffractogram of the product of the reaction with $\delta = 1$ could not initially be understood. We therefore carried out a single-crystal structure analysis using the Smart Apex CCD (Bruker), which led to a successful structure solution of a new type of structure, realized in $Zr_{10.4}V_{0.6}Sb_{18}$ (see Structure Determination).

Since this formula is less V-rich than the starting mixture, it is concluded that this structure cannot comprise any more vanadium. To check for the phase width at the Zr-rich border, we arc-melted a mixture of α-$ZrSb_2$ and Zr with a Zr:Sb ratio of 11:18. The reaction products contained the same structure in high yields (besides small amounts of α-$ZrSb_2$ and ZrSb), as shown by its powder diffraction and as proven by a second structure analysis. These antimonides do not decompose visibly in air over a period of several weeks. The powdered samples are metallic gray, and the well-shaped crystals have a silver luster.

For physical property measurements, phase-pure $Zr_{11}Sb_{18}$ was prepared in a Ta tube at 1200 °C as described above. The reaction products were checked for impurities and for the presence of the elements desired by EDS analyses (LEO 1530, with integrated EDAX Pegasus 1200) on selected crystals. No impurity atoms were found. The averaged atomic ratios of selected crystals of the samples containing $Zr_{11}Sb_{18}$ and $Zr_{10.4}V_{0.6}Sb_{18}$ were Zr:Sb = 35:65 and Zr:V:Sb = 33:1:66, respectively (all in atom percent), compared to the hypothetical values of 38:62 and 36:2:62. The V−K peak was visible, but its quantitative integration is questionable due to its small deviation from the background.

Table 1. Crystallographic Data for $Zr_{11}Sb_{18}$ and $Zr_{10.4}V_{0.6}Sb_{18}$

empirical formula	$Zr_{11}Sb_{18}$	$Zr_{10.37(4)}V_{0.63}Sb_{18}$
fw	3194.92	3169.34
T of data collection/K	295	295
space group, no.	$I\bar{4}2d$, 122	$I\bar{4}2d$, 122
a/pm	676.94(4)	676.48(8)
c/pm	6007.3(5)	6005.6(9)
V/(10^6 pm^3)	2752.8(3)	2748.3(6)
Z	4	4
calcd density/(g cm^{-3})	7.71	7.66
abs coeff/cm^{-1}	212.6	212.7
$R(F)$,[a] $R_w(F^2)$[b]	0.0599, 0.0891	0.0479, 0.0662

[a] $R(F) = \sum||F_o| - |F_c||/\sum|F_o|$. [b] $R_w(F^2) = [\sum[w(F_o^2 - F_c^2)^2]/\sum[w(F_o^2)^2]]^{1/2}$.

Table 2. Positional Parameters and Equivalent Displacement Parameters

atom	site	x[a]	y[a]	z[a]	U_{eq}/pm^2 [a]	U_{eq}/pm^2 [b]
Sb(1)	16e	0.3213(2)	0.3424(3)	0.4575(1)	9(1)	11(1)
Sb(2)	16e	0.3386(2)	0.1697(2)	0.693(1)	13(1)	14(1)
Sb(3)	16e	0.1538(3)	0.2071(2)	0.4035(1)	12(1)	15(1)
Sb(4)	16e	0.2236(3)	0.3459(3)	0.0151(1)	18(1)	18(1)
Sb(5)	8d	0.1571(4)	1/4	1/8	20(1)	21(1)
Zr(1)	8c	0	0	0.3629(1)	8(1)	9(1)
Zr(2)	8c	0	0	0.0889(1)	7(1)	8(1)
Zr(3)	4a	0	0	0	5(1)	7(1)
Zr(4)[c]	8c	0	0	0.4522(1)	10(1)	10(1)
Zr(5)[d]	8c	0	0	0.1829(1)	12(1)	14(1)
Zr(6)[e]	8c	0	0	0.2738(1)	10(1)	6(1)

[a] $Zr_{11}Sb_{18}$. [b] $Zr_{10.4}V_{0.6}Sb_{18}$. [c] Occupancy in $Zr_{10.4}V_{0.6}Sb_{18}$: 0.958(7)% Zr, 0.042% V. [d] Occupancy in $Zr_{10.4}V_{0.6}Sb_{18}$: 0.886(6)% Zr, 0.114% V. [e] Occupancy in $Zr_{10.4}V_{0.6}Sb_{18}$: 0.843(7)% Zr, 0.157% V.

Structure Determination. First, a prismatic-shaped single crystal of dimensions 50 × 45 × 30 μm, taken from the reaction aiming at hypothetical "Zr_4VSb_8", was mounted on a Smart Apex CCD diffractometer using Mo Kα radiation. Three sets of frames were collected with 0.3° scans in ω for exposure times of 60 s per frame. The data were corrected for Lorentz and polarization effects. The structure solution (SHELTXL package)[15] was successful in the tetragonal space group $I\bar{4}2d$, in agreement with the systematic absences. The resulting electron density map consisted of eleven peaks, five of which were assigned to be Sb atoms on the basis of their coordination spheres. The resulting six positions were all refined as being mixed occupied by Zr and V atoms, a strategy which revealed three sites occupied solely by Zr and three by different Zr/V mixtures. In any case, the V contributions were rather small, namely, 0%, 4%, 11%, and 16%. This model yielded uniform displacement parameters as well as reasonable residual factors (e.g., $R_w(F^2) = 6.6\%$). The data for the crystal structure of the binary $Zr_{11}Sb_{18}$ were collected and treated in the same way. Allowing for deficiencies on the Zr sites did not result in significant deviations from 100% occupancies. Crystallographic details can be found in Table 1. Positional parameters, equivalent displacement parameters, and occupancy factors are listed in Table 2. More details are given in the CIF file (see the Supporting Information).

(8) Völlenkle, H.; Wittmann, A.; Nowotny, H. *Monatsh. Chem.* **1966**, *97*, 506.
(9) Völlenkle, H.; Preisinger, A.; Nowotny, H.; Wittmann, A. *Z. Kristallogr.* **1967**, *124*, 9.
(10) Flieher, G.; Völlenkle, H.; Nowotny, H. *Monatsh. Chem.* **1968**, *99*, 2408.
(11) Kleinke, H. *Chem. Commun. (Cambridge)* **1998**, 2219.
(12) Kleinke, H. *J. Mater. Chem.* **1999**, *9*, 2703.
(13) Garcia, E.; Corbett, J. D. *J. Solid State Chem.* **1987**, *73*, 452.
(14) Kjekshus, A. *Acta Chem. Scand.* **1972**, *26*, 1633.
(15) Sheldrick, G. M. SHELXTL-V5.1, University of Göttingen, Göttingen, Germany, 1998.

Table 3. Selected Interatomic Distances *d* (pm) and −ICOHPs (eV per Bond)

contact	no.	*d* in $Zr_{11}Sb_{18}$	−ICOHP in $Zr_{11}Sb_{18}$	*d* in $Zr_{10.4}V_{0.6}Sb_{18}$
Sb(1)−Sb(2)	1	310.7(2)	0.49	311.9(1)
Sb(1)−Sb(1)	1	322.6(3)	0.19	325.2(2)
Sb(1)−Sb(4)	1	326.6(3)	0.32	325.8(2)
Sb(2)−Sb(1)	1	310.7(2)	0.49	311.9(1)
Sb(2)−Sb(2)	1	317.1(2)	0.26	316.7(2)
Sb(2)−Sb(3)	1	321.3(2)	0.22	321.9(2)
Sb(3)−Sb(2)	1	321.3(2)	0.22	321.9(2)
Sb(3)−Sb(5)	1	335.2(2)	0.21	334.5(2)
Sb(4)−Sb(1)	1	326.6(3)	0.32	325.8(2)
Sb(5)−Sb(3)	2	335.2(2)	0.21	334.5(2)
Zr(1)−Sb(3)	2	290.2(2)	1.67	291.2(1)
Zr(1)−Sb(5)	2	296.3(2)	1.42	297.1(2)
Zr(1)−Sb(3)	2	299.9(3)	1.39	298.8(2)
Zr(1)−Sb(2)	2	305.9(3)	1.26	307.0(2)
Zr(1)−Zr(1)	2	368.37(1)	0.46	367.6(2)
Zr(1)−Zr(2)	2	367.9(1)	0.41	367.8(1)
Zr(2)−Sb(2)	2	282.1(2)	1.66	282.6(2)
Zr(2)−Sb(5)	2	295.0(2)	1.32	294.0(2)
Zr(2)−Sb(3)	2	310.4(2)	1.19	310.6(1)
Zr(2)−Sb(1)	2	321.8(3)	0.76	322.8(2)
Zr(2)−Zr(5)	2	362.9(2)	0.28	362.6(1)
Zr(2)−Zr(1)	2	367.9(1)	0.41	367.8(1)
Zr(3)−Sb(4)	4	293.1(2)	1.57	292.0(1)
Zr(3)−Sb(1)	4	302.1(1)	1.32	302.8(1)
Zr(3)−Zr(6)	4	367.5(1)	0.42	367.83(9)
Zr(4)−Sb(2)	2	280.3(2)	1.38	280.3(2)
Zr(4)−Sb(4)	2	291.0(3)	1.24	290.8(2)
Zr(4)−Sb(1)	2	319.4(2)	0.43	317.8(1)
Zr(4)−Sb(3)	2	340.8(3)	0.26	341.8(2)
Zr(4)−Zr(5)	2	357.7(1)	0.15	358.1(1)
Zr(4)−Zr(6)	2	367.9(2)	0.18	366.6(1)
Zr(5)−Sb(1)	2	283.7(2)	1.30	282.3(2)
Zr(5)−Sb(3)	2	285.4(2)	1.57	284.4(2)
Zr(5)−Sb(2)	2	320.5(1)	0.50	320.31(8)
Zr(5)−Sb(4)	2	362.5(2)	0.08	363.9(2)
Zr(5)−Zr(4)	2	357.7(1)	0.15	358.1(1)
Zr(5)−Zr(2)	2	362.9(2)	0.28	362.6(1)
Zr(6)−Sb(1)	2	284.6(2)	1.50	284.7(1)
Zr(6)−Sb(4)	2	297.2(3)	1.25	298.0(2)
Zr(6)−Sb(4)	2	304.3(2)	1.24	303.8(1)
Zr(6)−Sb(2)	2	316.0(3)	0.90	314.0(2)
Zr(6)−Zr(3)	2	367.5(1)	0.42	366.6(1)
Zr(6)−Zr(4)	2	367.9(2)	0.18	367.83(9)

Band Structure Calculations. Self-consistent tight-binding LMTO calculations (LMTO = linear muffin tin orbital)[16−18] were carried out on the structure of $Zr_{11}Sb_{18}$. Therein, the density functional theory was used with the local density approximation (LDA). The integration in *k* space was performed by an improved tetrahedron method[19] on a grid of 568 *k* points of the first Brillouin zone (crystal orbital Hamiltonian populations (COHPs),[20] 292 *k* points). The integrated values (ICOHPs) are included in Table 3.

Physical Property Measurements. The Seebeck coefficients of $Zr_{11}Sb_{18}$ were determined on a cold-pressed bar (dimensions 5 × 1 × 1 mm) between 300 and 600 K using the commercial device from MMR Technologies.

Results and Discussion

Uncovery of $Zr_{11}Sb_{18}$. To us, it is most fascinating to realize that new binary transition-metal antimonides, which are thermodynamically stable with respect to the other antimonides in the phase diagram, can still be found with conventional solid-state methods. The only hint toward the existence of $Zr_{11}Sb_{18}$ was given by Corbett et al., who reported having found a new phase in the binary Zr−Sb system with an approximate Zr:Sb ratio of 2:3.[21] While the tentatively assigned lattice dimensions (tetragonal primitive, a = 956.6(2) pm, c = 528.8(1) pm) and stoichiometry ("Zr_2Sb_3") differ from our results, it is concluded that these authors found the same compound as evident from comparisons of the X-ray powder diffractograms, but were not able to identify $Zr_{11}Sb_{18}$ due to the lack of single crystals suitable for X-ray structure determinations. There is no relation between the herewith-determined unit cell and the tentatively assigned one, indicating that the first indexation was not correct.

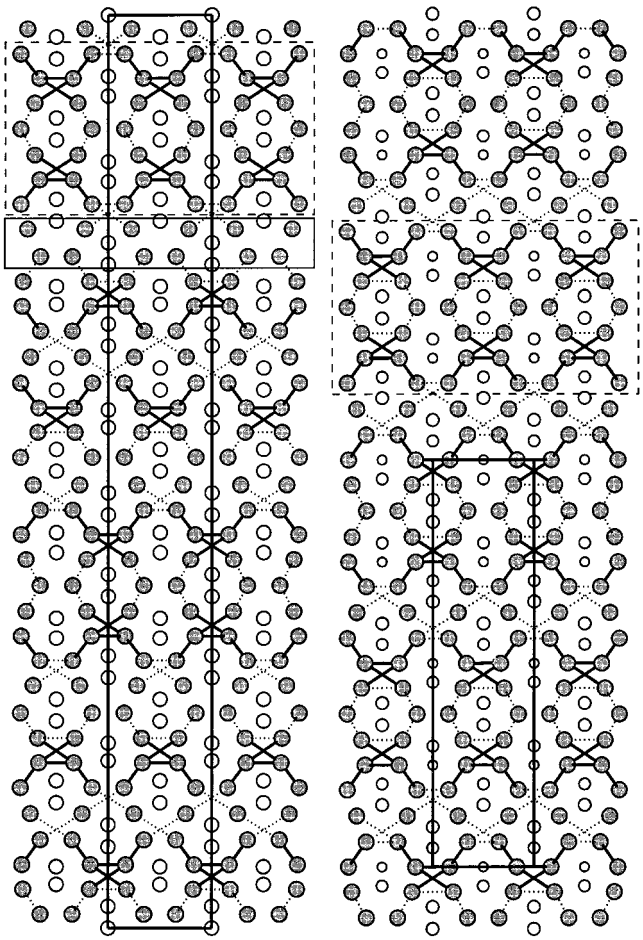

Figure 1. Projections of the structures of $Zr_{11}Sb_{18}$ (left) and $(Zr,Ti)_5Sb_8$ (right) along [100]: vertical, *c* axes; large, gray circles, Sb; small, white circles, M atoms; fat lines, Sb−Sb bonds <322 pm. M−Sb bonds are omitted for the sake of clarity.

Crystal Structure of $Zr_{11}Sb_{18}$. 1. Structure Description. Figure 1 illustrates the comparison between the crystal structure of $Zr_{11}Sb_{18}$, a new type of structure, and the recently published structure of M_5Sb_8 (M = Ti, Zr, Nb, Mo).[7] Only the homonuclear M−M and Sb−Sb contacts are emphasized, for showing the multitude of the dominating M−Sb interactions would result in a too complex figure.

(16) Andersen, O. K., Barth, U.; van Hedin, L. *J. Phys.* **1971**, *C4*, 2064.
(17) Andersen, O. K. *Phys. Rev.* **1975**, *B12*, 3060.
(18) Skriver, H. L. *The LMTO Method*; Springer: Berlin, 1984.
(19) Blöchl, P. E.; Jepsen, O.; Andersen, O. K. *Phys. Rev.* **1994**, *B49*, 16223.
(20) Dronskowski, R.; Blöchl, P. *J. Phys. Chem.* **1993**, *97*, 8617.
(21) Garcia, E.; Corbett, J. D. *J. Solid State Chem.* **1987**, *73*, 440.

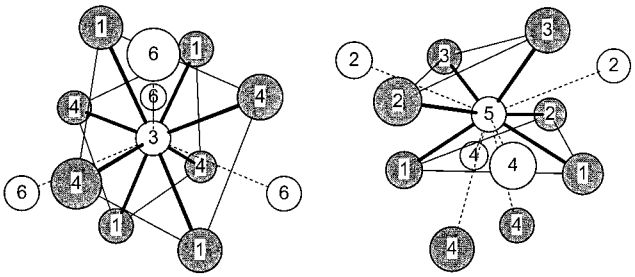

Figure 2. Coordination spheres around Zr(3) (left) and Zr(5) (right) of $Zr_{11}Sb_{18}$.

The structure of M_5Sb_8 is comprised of Sb_6 units (emphasized via fat lines) interconnected by an additional Sb atom via longer Sb−Sb contacts. This three-dimensional Sb atom network includes the M atoms, which themselves form a three-dimensional network with larger interatomic distances (omitted in Figure 1). Similar structure features were found in some late-transition-metal silicides, germanides, and stannides, e.g., in $Mn_{27}Si_{47}$,[22] Ir_4Ge_5,[23] and Ru_2Sn_3.[24]

The very same unit occurs in the structure of $Zr_{11}Sb_{18}$, for the dashed rectangles in both parts of Figure 1 represent topologically equivalent parts of the two different structures. It is evident that the $Zr_{11}Sb_{18}$ structure is closely related to the $(Zr,Ti)_5Sb_8$ structure, which exists up to the high Zr:Ti ratio of 3.9(3):1.1. It is noted that the metal:Sb ratio is almost the same in these two similar yet distinctly different structures: the antimony content varies only slightly between 62.1 atom % in $Zr_{11}Sb_{18}$ and 61.5 atom % in $Zr_{3.9}Ti_{1.1}Sb_8$. The higher Sb content in $Zr_{11}Sb_{18}$ is reflected in a new structure motif not found in $Zr_{3.9}Ti_{1.1}Sb_8$, which is indicated by the solid rectangle in the left part of Figure 1.

However, this description based on interwoven Zr and Sb atom networks shall not imply that the homonuclear interactions are the strongest here; quite the opposite is the case. In the structure of $Zr_{11}Sb_{18}$, each Zr atom is surrounded by eight Sb atoms at distances starting at 280 pm, while the shortest Sb−Sb and Zr−Zr contacts are 311 and 358 pm, respectively. Selected interatomic distances are presented in Table 3 ($d_{Zr-Sb} < 370$ pm, $d_{Zr-Zr} < 370$ pm, and $d_{Sb-Sb} < 350$ pm).

2. Zr−Sb Interactions. As seen in Figure 1, all Zr atoms have very similar coordination spheres, each atom being surrounded by eight Sb atoms and four Zr atoms. The most significant differences occur in the ranges of Zr−Sb distances *d*, which may be as small as 10 pm for Zr(3) (left part of Figure 2, $d_{Zr(3)-Sb} = 293$ and 302 pm) and as large as 80 pm for Zr(5) (right part of Figure 2, $d_{Zr(5)-Sb} = 284$, 285, 321, and 363 pm). While there are many Zr−Sb distances on the order of 310−320 pm, the two long Zr(5)−Sb(4) distances of 363 pm (dashed lines in Figure 2) stand out and might be neglected in a first approximation. Then, Zr(5) is surrounded by six Sb atoms, forming a distorted octahedron (emphasized are two opposite, staggered triangular faces via thin solid lines in the right part of Figure 2). On the other hand, the other Zr atoms are located in Sb_8 polyhedra, which are reminiscent of square antiprisms. One example is Zr(3): the Sb atoms in front of the left part of Figure 2 (large circles, numbers 1 (2×) and 4 (2×)) occupy the vertexes of the upper quadrangle, and the smaller circles (again numbers 1 (2×) and 4 (2×)) form the lower quadrangle staggered with respect to the upper one—as indicated with the thin solid lines between the vertexes. Zr(4) represents an intermediate case, with Zr−Sb distances of 280, 291, 319, and 341 pm, each occurring twice per Zr(4) atom.

The coordination spheres of the M atoms in $Zr_\delta Ti_{5-\delta}Sb_8$ ($1.1 \le \delta \le 3.9$) resemble those occurring in $Zr_{11}Sb_{18}$. Therein, two M sites have eight Sb neighbors (273−334 pm), and the third one is six-coordinated with M−Sb bonds between 274 and 315 pm. The M−Sb distances increase with increasing Zr content, for Zr atoms are significantly larger than Ti atoms (Pauling single bond radii, $r_{Ti} = 132$ pm, $r_{Zr} = 145$ pm;[25] Slater's empirical atomic radii, $r_{Ti} = 140$ pm, $r_{Zr} = 155$ pm).[26] In addition, the Zr atoms prefer the sites with higher coordination numbers in $Zr_\delta Ti_{5-\delta}Sb_8$. The slightly higher averaged M−Sb coordination in $Zr_{11}Sb_{18}$, compared to M_5Sb_8 (7.64 vs. 7.60, ignoring all M−Sb distances >350 pm), most likely contributes to the preferred formation of the $Zr_{11}Sb_{18}$ structure in the binary Zr−Sb system.

The shorter Zr−Sb distances in $Zr_{11}Sb_{18}$ are on the order of the sum of Pauling's single bond radii, namely, $r_{Zr} + r_{Sb} = 145$ pm + 140 pm = 285 pm,[25] which is indicative of strong covalent Zr−Sb bonds. Comparable bonds are found in the other binary zirconium antimonides: e.g., in ZrSb, the Zr atoms are surrounded by seven or five Sb atoms at distances between 284 and 291 pm, and in α-$ZrSb_2$, the two different Zr atoms are bonded to eight and nine Sb atoms with contacts between 294 and 345 pm. The structure of β-$ZrSb_2$ ($PbCl_2$ type), which was reported to be slightly Sb-deficient (i.e., $ZrSb_{1.96}$), comprises $ZrSb_9$ polyhedra with Zr−Sb bonds between 292 and 321 pm.[13] Thus, the multitude of Zr−Sb bonds per Zr atom increases smoothly from ZrSb (5−7) over $Zr_{11}Sb_{18}$ (6−8) to $ZrSb_2$ (8−9), which is deduced to arise from the increasing Sb content in this series.

3. Zr−Zr Interactions. The opposite trend—as expected—becomes apparent by comparing the Zr−Zr bonds, which decrease among the binary zirconium antimonides with increasing Sb ratio. The two different Zr atoms in ZrSb form three and four Zr−Zr bonds of 339 and 340 pm, and only one of the two Zr atoms in $ZrSb_2$ takes part in one Zr−Zr bond of 344 pm, compared to the four (longer) Zr−Zr distances per Zr atom in $Zr_{11}Sb_{18}$ from 358 to 368 pm. A similar yet smaller range was found in the structure of $Zr_{3.9}Ti_{1.1}Sb_8$ (357−364 pm), reflecting the size differences between Ti and Zr atoms. All of these interactions are presumably weakly bonding, compared to Zr−Zr single bonds (i.e., twice the Zr radius = 290 pm) and the Zr−Zr bonds in elemental zirconium (hexagonal closed packed

(22) Zwilling, G.; Nowotny, H. *Monatsh. Chem.* **1973**, *104*, 668.
(23) Flieher, G.; Völlenkle, H.; Nowotny, H. *Monatsh. Chem.* **1968**, *99*, 877.
(24) Schwomma, O.; Nowotny, H.; Wittmann, A. *Monatsh. Chem.* **1964**, *95*, 1538.
(25) Pauling, L. *The Nature of the Chemical Bond*, 3rd ed.; Cornell University Press: Ithaca, NY, 1948.
(26) Slater, J. C. *J. Phys. Chem.* **1964**, *41*, 3199.

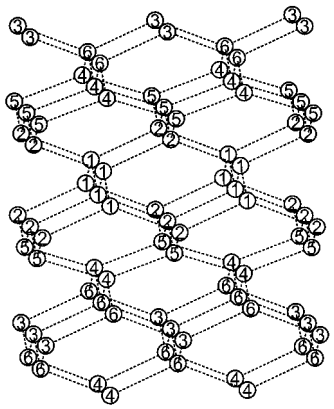

Figure 3. Diamond-like Zr atom network of $Zr_{11}Sb_{18}$.

modification, hcp-Zr, six bonds of 318 pm and six bonds of 323 pm; body-centered cubic modification, bcc-Zr, eight bonds of 309 pm and six bonds of 357 pm). This will be discussed in more detail in the paragraphs dealing with the electronic structure of $Zr_{11}Sb_{18}$.

In the case of $Zr_{11}Sb_{18}$, all Zr atoms are situated in (distorted) Zr_4 tetrahedra that are interconnected via common vertexes to form a diamond-like network (Figure 3). In addition to the occurrence of different Zr−Zr bond lengths, the bond angles vary very significantly between 97° and 142°. These deviations from the ideal tetrahedra are slightly larger than in the case of $Zr_{3.9}Ti_{1.1}Sb_8$ with bond angles between 98° and 139°. This is also reflected in similar deviations from the ideal *c*/*a* ratio, which is equal to 1 in diamond, but is calculated to be $6007.3/(11 \times 676.94) = 0.81$ in $Zr_{11}Sb_{18}$ and $2679.7/(5 \times 671.06) = 0.80$ in $Zr_{3.9}Ti_{1.1}Sb_8$.

4. Sb−Sb Interactions. Since bonding Sb−Sb interactions are present even in the more Zr-rich binary antimonide ZrSb,[13] we expected to find stronger ones in the structure of $Zr_{11}Sb_{18}$. ZrSb is the most Zr-rich binary zirconium antimonide with Sb−Sb bonds, which are 324 and 325 pm in length within a puckered Sb atom layer of hexagons. α-$ZrSb_2$ comprises several shorter Sb−Sb bonds with lengths between 289 and 310 pm. This shorter bond of 289 pm may be compared to typical single bonds, as found in KSb (283−285 pm)[27] or in molecular units such as cyclo-Sb_5^{5-} (281−291 pm)[28] and Sb_{11}^{3-} (276−285 pm).[29] The intermediate ones on the order of 310 pm are often referred to as half-bonds (i.e., having a bond order of 1/2),[30−32] as most recently reinforced by an investigation of the electronic structure of $ZrSb_2$.[33] The shortest Sb−Sb distances in $Zr_{11}Sb_{18}$ occur in an "anchor-like" Sb_6 unit (comprising Sb(1), Sb(2), and Sb(3), Figure 4) with Sb−Sb distances between 311 and 321 pm, which may also be regarded as half-bonds.

A topologically equivalent Sb_6 unit (consisting of Sb(1) and Sb(2), right part of Figure 5) was found in the structure

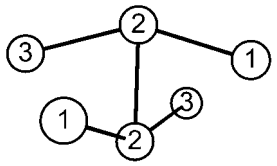

Figure 4. $(Sb(1)-Sb(2)\text{-}Sb(3))_2$ anchor-like unit of $Zr_{11}Sb_{18}$.

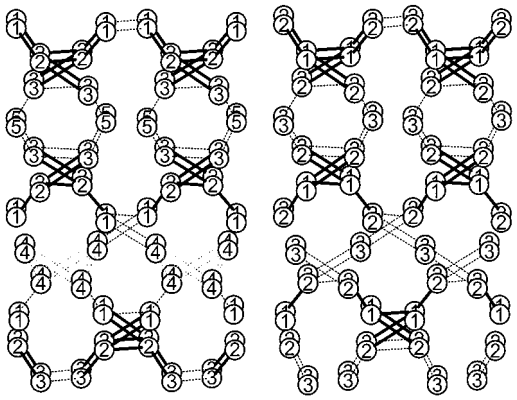

Figure 5. Sb atom substructures of $Zr_{11}Sb_{18}$ (left) and $(Zr,Ti)_5Sb_8$ (right).

of $Zr_{3.9}Ti_{1.1}Sb_8$, with Sb−Sb bonds of 319 pm. There, these units are interconnected via an additional Sb atom (Sb(3)), forming significantly longer Sb−Sb contacts of 334 pm, as well as by direct contacts between neighboring "anchors" (340 pm) to a three-dimensional extended Sb atom substructure. The same connections exist in the structure of $Zr_{11}Sb_{18}$ with distances of 327 pm between the Sb_6 anchors and the additional atom (Sb(5), left part of Figure 5) and 323 pm between two neighboring anchors. It is noted that the differences of the interatomic distances within and between the anchors (311−321 pm vs 323−327 pm) are much smaller in $Zr_{11}Sb_{18}$ compared to $(Zr,Ti)_5Sb_8$; however, it is at least mnemonically useful to continue using the description based on Sb_6 anchors. The prototype is realized in the structure of Ru_2Sn_3,[24] whose Sn atom substructure consists entirely of such anchors, with Sn−Sn distances between 309 and 312 pm. However, no related structures occur in the early-transition-metal stannides or antimonides; e.g., Ti_2Sn_3 forms a completely different structure.[34]

As revealed in Figure 5, further Sb atoms (Sb(4)) occur between the Sb_6 units along the *c* axis that are not present in $Zr_{3.9}Ti_{1.1}Sb_8$, with nonetheless (at least in part) significant Sb−Sb contacts ($d_{Sb(1)-Sb(4)} = 327$, $d_{Sb(4)-Sb(4)} = 353$ pm). The Sb(4)−Sb(4) distance stands out compared to the series of the other Sb−Sb distances in $Zr_{11}Sb_{18}$ that range between 311 and 327 pm. As discussed above, classical bonds of 280−290 pm are considered to be full bonds (single bonds, i.e., two electrons per bond), those around 310 pm are treated as half-bonds (one electron per bond), and contacts on the order of 335 pm, as in elemental antimony, as (not precisely defined) weak bonds—in contrast to van der Waals interactions that might start around 350 pm.[33,35−37] Thus, the

(27) Hönle, W.; von Schnering, H.-G. *Z. Kristallogr.* **1981**, *155*, 307.
(28) Korber, N.; Richter, F. *Angew. Chem., Int. Ed. Engl.* **1997**, *36*, 1512.
(29) Bolle, U.; Tremel, W. *J. Chem. Soc., Chem. Commun.* **1992**, 91.
(30) Ferguson, M. J.; Hushagen, R. J.; Mar. A. *J. Alloys Compd.* **1997**, *249*, 191.
(31) Kleinke, H. *Eur. J. Inorg. Chem.* **1998**, 1369.
(32) Papoian, G. A.; Hoffmann, R. *Angew. Chem., Int. Ed.* **2000**, *39*, 2408.
(33) Papoian, G. A.; Hoffmann, R. *J. Am. Chem. Soc.* **2001**, *123*, 6600.
(34) Kleinke, H.; M. Waldeck, M.; Gütlich, P. *Chem. Mater.* **2000**, *12*, 2219.
(35) Pykkö, P. *Chem. Rev.* **1997**, *97*, 597.
(36) Kleinke, H. *Inorg. Chem.* **1999**, *38*, 2931.
(37) Kleinke, H. *Chem. Soc. Rev.* **2000**, *29*, 411.

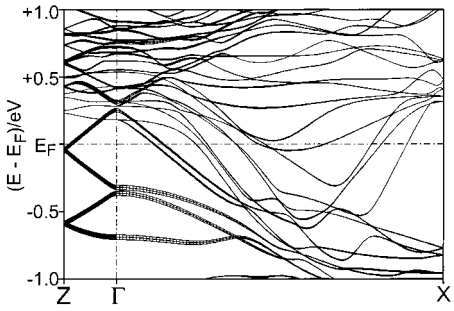

Figure 6. Band structure of $Zr_{11}Sb_{18}$. Zr $d_{x^2-y^2}$ contributions are emphasized via fat band representation.

character of the longer Sb(4)−Sb(4) interaction (353 pm) remains questionable here. One might therefore consider the Sb atom substructure as being extended only along two directions, namely, along the *a* and *b* axes, which are equivalent by symmetry because of the tetragonal crystal system. More insight was gained after the electronic structure was calculated—especially the COHPs[20] as discussed below.

Electronic Structure of $Zr_{11}Sb_{18}$. For more sophisticated discussions we calculated the band structure of $Zr_{11}Sb_{18}$ and extracted information regarding the densities of states (DOSs) and COHPs. In the crystal orbital Hamiltonian populations, the densities of states are weighted according to the bonding and antibonding contributions, comparable to the crystal orbital overlap populations (COOPs)[38] used in extended Hückel calculations.[39,40] Both methods allow for comparisons of relative bond strengths.

The band structure is shown in Figure 6 along the two selected symmetry lines $Z \rightarrow \Gamma$ and $\Gamma \rightarrow X$, i.e., parallel to c^* and a^*, respectively.[41] Several bands with mostly Zr d character cross the Fermi level, E_F, between Γ and *X*, giving raise to metallic properties along two directions because of the tetragonal symmetry. Exactly one band crosses E_F along $\Gamma \rightarrow Z$ with main contributions of the $d_{x^2-y^2}$ orbitals of all Zr atoms, as indicated via the *fat band*[42] representation. However, since band gaps along $\Gamma \rightarrow Z$ are present in the vicinity of E_F, it should be possible to reduce the metallic properties to two dimensions by reducing the valence-electron concentration of $Zr_{11}Sb_{18}$. This may be achieved by partial replacements of Sb by Sn atoms or of Zr by Sc atoms. The successful synthesis of $Zr_{10.4}V_{0.6}Sb_{18}$ shows that the valence-electron concentration can be changed (at least increased) to some extent.

The DOSs and the projections onto the Zr and Sb atoms are shown in the left part of Figure 7. The lower peak between −8 and −13 eV stems from Sb 5s states, with some minor contribution of Zr due to the covalence of the Zr−Sb interactions. The peak above −6 eV, the conduction band, consists primarily of Sb 5p states (concentrated between −1 and −6 eV) and Zr 4d states, which dominate the region above −1 eV. There is no gap between the peaks dominated by Sb and Zr contributions, just a not very pronounced minimum. Therefore, no modifications of $Zr_{11}Sb_{18}$ could help in achieving good bulk thermoelectric properties, for that would require the formation of a (pseudo)gap. This is in contrast to the situation in the electronic structure of M_5Sb_8.[7] However, one-dimensional good thermoelectric properties should be achievable by reducing the valence-electron concentration.

Undoubtedly, the strongest stabilization comes from the Zr−Sb bonding, which is depicted in the middle of Figure 7. This was expected on the basis of the multitude of short Zr−Sb contacts in the structure of $Zr_{11}Sb_{18}$. Only bonding states are filled, and raising the Fermi level (as done with the incorporation of V atoms in lieu of Zr atoms) by up to 1 eV would increase the Zr−Sb bonding interactions by filling more bonding states.

The homonuclear interactions (right part of Figure 7) are apparently of less importance but still significantly bonding. Note that the interactions of the given kinds Zr−Sb, Zr−Zr, and Sb−Sb were all cumulated over the whole cell, and that the scales for the COHPs were chosen differently as to make the less strong COHPs visible; i.e., the scale of the heteronuclear Zr−Sb interactions is 10 times larger than that of the homonuclear ones.

As is the case for the Zr−Sb bonds, only bonding Zr−Zr states are situated below E_F, which become antibonding above 2 eV. Then, again, raising E_F would increase the bonding interactions. On the other hand, both bonding and antibonding Sb−Sb states are filled in the structure of $Zr_{11}Sb_{18}$. Lowest in energy are the s orbitals with bonding contributions below −9.5 eV and antibonding ones between −8 and −9.5 eV, while the bonding interactions dominate. Similarly, the p orbitals participate in bonding interactions between −3 and −6 eV, and become antibonding at −3 eV. Below the Fermi level the antibonding p states are outweighed by the bonding p states such as in the case of the s block. Thus, the net contribution of the Sb−Sb interactions is of bonding character. Here, however, increasing the valence-electron configuration would occur with weakening of the Sb−Sb bonds because of more filled antibonding states.

To provide more details on the different interactions, all different ICOHPs are plotted vs the bond lengths in Figure 8. The literature available on ICOHPs is rather sparse. Some information regarding 3d transition metals was given by Landrum and Dronskowski, who calculated the ICOHPs for the strongest bonds in elemental iron (α-Fe, −1.53 eV per bond), cobalt (−1.22 eV per bond), and nickel (−1.00 eV per bond).[43] Most chemists are more familiar with the Mulliken overlap populations (MOPs),[44] which are the extended Hückel analogues to the ICOHPs obtained with the *first principles* LMTO method. Both parameters, the ICOHPs and the MOPs, are a measure of relative bond strengths. It must be noted that negative ICOHPs, but positive

(38) Hughbanks, T.; Hoffmann, R. *J. Am. Chem. Soc.* **1983**, *105*, 3528.
(39) Hoffmann, R. *J. Chem. Phys.* **1963**, *39*, 1397.
(40) Whangbo, M.-H.; Hoffmann, R. *J. Am. Chem. Soc.* **1978**, *100*, 6093.
(41) Bradley, C. J.; Cracknell, A. P. *The Mathematical Theory of Symmetry in Solids*; Clarendon Press: Oxford, 1972.
(42) Jepsen, O.; Andersen, O. K. *Z. Phys.* **1995**, *97*, 25.
(43) Landrum, G. A.; Dronskowski, R. *Angew. Chem., Int. Ed.* **2000**, *39*, 1560.
(44) Mulliken, R. S. *J. Chem. Phys.* **1955**, *23*, 2343.

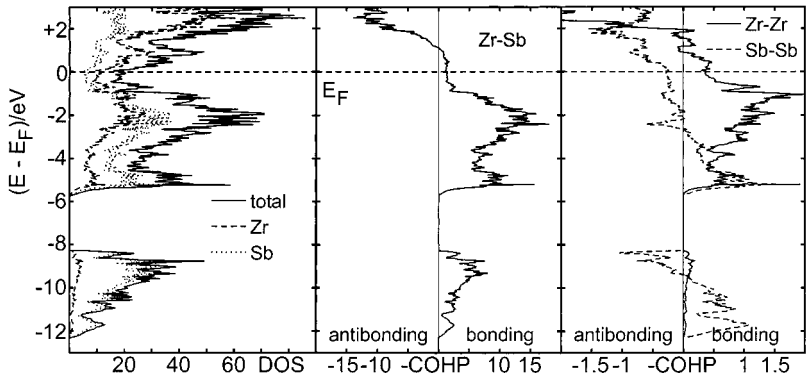

Figure 7. DOSs (left) and Zr−Sb (middle), and Zr−Zr as well as Sb−Sb (both right) COHPs of $Zr_{11}Sb_{18}$.

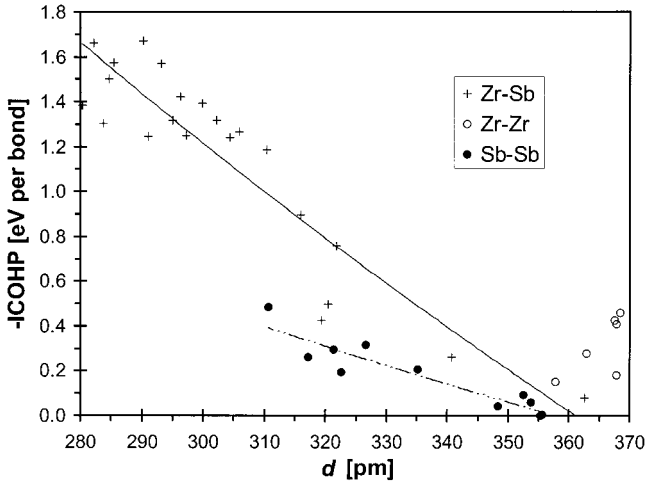

Figure 8. −ICOHPs of $Zr_{11}Sb_{18}$.

MOPs, indicate bonding interactions. For simplicity we will multiply all ICOHP values by −1, and subsequently note those values as −ICOHPs.

While all interactions depicted in Figure 8 exhibit net bonding character, the dominance of the Zr−Sb bonds in Figure 8 is evident. One might set a cutoff for the Zr−Sb bonds at 350 pm, for the one at 363 pm with an ICOHP = −0.08 eV per bond (i.e., −ICOHP = 0.08 eV per bond) is negligible compared to the shorter ones, which can have −ICOHPs as high as 1.67 eV per bond, with the majority being above 1.20 eV per bond. A similar cutoff for significant Sb−Sb distances would be set at 340 pm; the shorter bonds have −ICOHPs between 0.49 and 0.21 eV per bond, the longer ones (all above 350 pm) exhibit much smaller values (<0.1 eV per bond). On the other hand, the Zr−Zr interactions between 358 and 368 pm are all significantly bonding with −ICOHPs between 0.15 and 0.46 eV per bond. The logarithmic trendlines indicated for the Zr−Sb and Sb−Sb bonds show the differences in the dependence of bond length and strength, while the number of data points for the Zr−Zr interaction is not sufficient to create a reasonable trendline.

To gain more understanding of these −ICOHP values, we compare MOPs (calculated in our group, mostly introduced before)[37,45] and −ICOHPs of selected Zr−Zr and Sb−Sb bonds of different compounds in Tables 4 and 5. For example, the eight short Zr−Zr bonds in cubic body-centered zirconium (309 pm) exhibit an MOP of 0.29 electrons per bond and a −ICOHP of 1.45 eV per bond. In most cases, the bond strengths decrease with decreasing distances, as do the MOPs and −ICOHPs. In all of the cases the −ICOHPs are significantly higher than the MOPs—when the different units are ignored. We state that significantly bonding Zr−Zr interactions are present in all binary zirconium antimonides, which decrease with decreasing Zr content as postulated above. Even the longer contacts of 368 pm still have significant −ICOHPs (and MOPs) on the order of a third of those in hexagonal zirconium.

Table 4. MOPs (Electrons per Bond) and −ICOHPs (eV per Bond) for Selected Zr−Zr Bonds

compd	*d*/pm	MOP	−ICOHP
bcc-Zr	309, 357	0.29, 0.15	1.45, 0.68
hcp-Zr	318, 323	0.27, 0.25	1.30, 1.25
ZrSb	339, 340	0.15, 0.18	0.86, 0.46
$Zr_{11}Sb_{18}$	358−368	nc	0.15−0.46
$ZrSb_2$	344	0.09	0.78

Table 5. MOPs (Electrons per Bond) and −ICOHPs (eV per Bond) for Selected Sb−Sb Bonds

compd	*d*/pm	MOP	−ICOHP
KSb	283, 285	0.66, 0.63	2.29, 1.87
Sb	291, 336	0.53, 0.08	1.63, 0.26
La_3TiSb_5	314	0.26	0.62
ZrSb	324, 325	0.06, 0.09	0.09, 0.14
$Zr_{11}Sb_{18}$	311−335	nc	0.49−0.21
$ZrSb_2$	289, 307−310	0.51, 0.12−0.29	1.21, 0.41−0.65

Full, classical Sb−Sb bonds (283 and 285 pm) were found in the Zintl-phase KSb (two bonds per Sb^- in a zigzag chain).[27] The −ICOHPs (2.29 and 1.87 eV per bond) are about 3 times larger than the MOPs (0.66 and 0.63 electrons per bond). A half-bond, as found in La_3TiSb_5,[30] has an MOP of 0.26 electrons per bond and a −ICOHP of 0.62 eV per bond, according to our calculations. The bonds in $Zr_{11}Sb_{18}$ are weaker (yet still significant) with −ICOHPs between 0.21 and 0.49 eV per bond despite their in part shorter lengths. Again, a comparison of the Sb−Sb interactions within the binary zirconium antimonides reveals an increase with increasing Sb content.

Physical Properties of $Zr_{11}Sb_{18}$. The temperature dependence of the Seebeck coefficient (thermopower) of $Zr_{11}Sb_{18}$ is shown in Figure 9. It varies slightly between 6 and 8 μV/K within the temperature range measured (300−600 K). These

(45) Kleinke, H. *J. Am. Chem. Soc.* **2000**, *122*, 853.

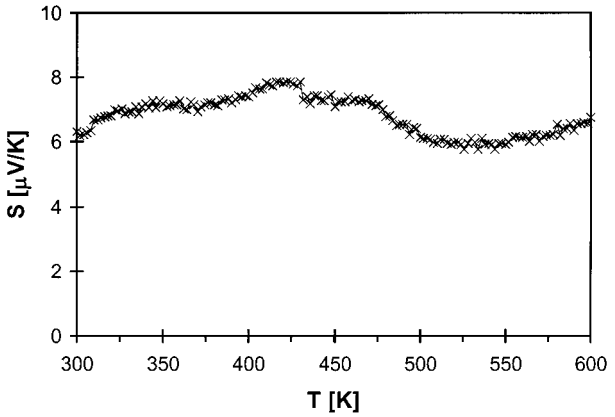

Figure 9. Thermopower of $Zr_{11}Sb_{18}$.

values are typical for (p-type) metals such as zirconium (8.9 μV/K at 300 K) and hafnium (5.5 μV/K).[46] The complex temperature dependence is indicative of several bonds contributing to the electronic transport properties, as predicted by the band structure (Figure 6).

Ternary Variant $Zr_{10.37(4)}V_{0.63}Sb_{18}$. A rather small phase range exists in $Zr_{11-\delta}V_{\delta}Sb_{18}$ with $0 \leq \delta \leq 0.63(4)$. The incorporation of V atoms in lieu of Zr atoms (6%) led to a slight contraction of the unit cell, i.e., 0.07% and 0.03% contractions of the *a* and *c* axes, respectively. This may be caused by the smaller size of the V atom (Pauling, $r_V = 122$ pm; Slater, $r_V = 135$ pm) and an increase in valence-electron concentration, leading to an increase in the bonding character of the M−Sb and M−M interactions, and a decrease of the Sb−Sb bonds. Correspondingly, most Sb−Sb bonds are longer by about 1 pm in $Zr_{10.4}V_{0.6}Sb_{18}$ despite its smaller unit cell, while the opposite is true for the M−M bonds. There is no clear trend for the M−Sb bonds, however. The slight increase in the number of valence electrons (Zr, 4; V, 5) cannot change the metallic properties. From the COHP curves, it became clear that the increase would occur with filling of the antibonding Sb−Sb states, which might cause the rather strict upper limit of the V atom incorporation.

(46) Vedernikow, M. V.; Dvunitkin, V. G.; Zhumagulov, A. *Fiz. Tverd. Tela* **1978**, *20*, 3302.

Conclusion

The new binary zirconium antimonide $Zr_{11}Sb_{18}$ and its ternary variant $Zr_{10.4}V_{0.6}Sb_{18}$ have been prepared and structurally characterized. $Zr_{11}Sb_{18}$ crystallizes in its own structure type, mainly stabilized by heteronuclear Zr−Sb bonds, while both homonuclear kinds, namely, Zr−Zr and Sb−Sb bonding, contribute significantly.

The structure of $Zr_{11}Sb_{18}$ contains a two-dimensional Sb atom network interwoven with a three-dimensional Zr atom network, which is strongly related to the structure of $Zr_{3.9}Ti_{1.1}Sb_8$ comprising a three-dimensional Sb atom network of the same anchor-like Sb_6 units. The Sb−Sb bonds in the Sb_6 anchors—the shortest in these structures—are considered to be nonclassical half-bonds, intermediate between those found in ZrSb and $ZrSb_2$.

$Zr_{11}Sb_{18}$ and $Zr_{10.4}V_{0.6}Sb_{18}$ are three-dimensional metallic conductors with small Seebeck coefficients. Reducing the valence-electron concentration should come along with low-dimensional metallic properties.

Acknowledgment. Financial support from the Natural Sciences and Engineering Research Council (NSERC), the Canada Foundation for Innovation (CFI), the Ontario Innovation Trust (OIT), and Materials and Manufacturing Ontario (MMO) is appreciated.

Supporting Information Available: One X-ray crystallographic file in CIF format. This material is available via the Internet at http://pubs.acs.org.

IC0108235